RSC Advances

PAPER

View Article Online
View Journal | View Issue



Cite this: *RSC Adv.*, 2020, **10**, 13286

# Projection method as a probe for multiplexing/demultiplexing of magnetically enriched biological tissues†

Mohammad Reza Zamani Kouhpanji [ab] and Bethanie J. H. Stadler *[ac]

Received 18th February 2020
Accepted 24th March 2020

DOI: 10.1039/d0ra01574a

rsc.li/rsc-advances

The unmet demand for cheap, accurate, and fast multiplexing of biomarkers has urged nanobiotechnology to prioritize the invention of new biomarkers that make feasible the remote detection, identification, and quantification of biological units, such as regenerative tissues. Here, we introduce a novel approach that highlights magnetic nanowires (MNWs) with such capabilities. This method employs the stable magnetization states of MNWs as a unique characteristic that can be realized by projecting the MNWs' switching field on the backward field ($P_{Hb}$), also known as the irreversible switching field. Experimentally, several types of MNWs were directly synthesized inside polycarbonate tissues and their $P_{Hb}$ characteristics were measured and analyzed. Our results show that the $P_{Hb}$ gives an excellent identification and quantification characteristic for demultiplexing MNWs embedded in these tissues. Furthermore, this method significantly improves the characterization speed by a factor of 50×–100× that makes it superior to the current state of the art that ceased the progression of magnetic nanoparticles in multiplexing/demultiplexing applications.



## Introduction

Progress of biological sciences substantially depends on biomarkers because they are the backbone of essential tools, such as optical microscopy and flow cytometry techniques, in this field.[1,2] However, surprisingly, none have offered the capabilities to mitigate the high-cost, high-complexity, and low-speed associated with these techniques.[3–6] Furthermore, there is still a lack of biomarkers that can be excited remotely and noninvasively with a single excitation source regardless of their surrounding tissues because almost all biomarkers under study to date are optical.[7–9]

The magnetic biomarkers, on the other hand, have potential to accelerate the progression of biological sciences. The current state of the arts in magnetic biomarkers is superparamagnetic iron oxide nanoparticles (IONs). These IONs have isotropic magnetic properties that restrict them from possessing distinct signatures that can be uniquely identified.[10,11] As a result, IONs have been limited in application to the enrichment of the biological entities with conjugation to optical biomarkers, such as fluorescent molecules, for readout.[12–15] Unfortunately, IONs also have weak magnetic properties that limit their use in ultralow enrichment and multiplexing applications.[7]

In this paper, we propose ferromagnetic nanowires (MNWs) as biomarkers for multiplexing applications. The special cylindrical geometry of MNWs gives rise to a well-defined magnetic anisotropy[16] that makes them suitable for many biological applications, such as MRI contrast, magnetic enrichment, and nanowarming.[11,17–21] An external field can be remotely used to physically excite MNWs, which makes them suitable for cell tracking,[22–25] cells manipulation,[26] cell separation,[27,28] drug delivery and drug activation,[29,30] magnetic hyperthermia,[21] and magneto-elastic ferrogels for tissue engineering.[31,32] Furthermore, the MNWs have shown a high internalization by cells in comparison to other magnetic nanoparticles, such as IONs, improving the enrichment and multiplexing yield.[26,28,33] As a consequence, MNWs have recently attracted attention as enrichment agents for studying breast and lung cancers,[34,35] CTCs,[36] and leukemia.[37]

Regardless of the tremendous opportunities for MNWs, they have not been used as self-standing biomarkers for multiplexing applications up to date due to three major drawbacks. First, magnetic characterization techniques are technically inefficient because they are slow. Second, the unique magnetic characteristics cannot unambiguously be measured due to the influence of external effects, such as para/diamagnetic response of the surrounding components. Third, the magnetic signatures of MNWs can overlap, which has limited their use as multiplexed biomarkers. To suppress these substantial obstacles, we propose a magnetic measurement technique that significantly

[a]*Department of Electrical and Computer Engineering, University of Minnesota Twin Cities, USA. E-mail: stadler@umn.edu; Tel: +1-612-626-1628*
[b]*Department of Biomedical Engineering, University of Minnesota Twin Cities, USA*
[c]*Department of Chemical Engineering and Materials Science, University of Minnesota Twin Cities, USA*

† Electronic supplementary information (ESI) available. See DOI: 10.1039/d0ra01574a

facilitates the detection of MNWs signature regardless of their surroundings.[10,38,39] Along with this, we establish a technique to quantitatively demultiplex the signature of multiple types of MNWs even though the individual signatures overlap.

Our methodology is based on our recently developed magnetic characterization method, named "projection method" that highly accelerates detection, identification, and quantification of MNWs regardless of their surroundings. A schematic of the projection method is shown in Fig. 1a.

Briefly, the projection method relays on measuring a few points next to the upper branch hysteresis loop (UBHL), shown as the black dots in Fig. 1a. Experimentally, the projection method measures the UBHL in a 2D format as a function of two fields, forward field ($H_f$) and backward field ($H_b$). The backward field is the descending field from positive saturation (point 1 in Fig. 1a) that sets the initial magnetization state of the MNWs (point 2 in Fig. 1a).

Then, the forward field is applied from the backward field to its previous backward field (point 3 in Fig. 1a) to slightly disturb the initial magnetization state of the MNWs. At this step, the field should be returned to the saturation field (point 1 in Fig. 1a) in one step before starting another backward field. The theoretical analysis of the projection method is given in the ESI.†

According to the inset in Fig. 1a, the projection method's protocol splits the derivative of the upper branch of the hysteresis loop (vertical distance between points 2 and 2′) into two parts that eliminates the extrinsic effects (the red arrow in Fig. 1a, RSF) from the intrinsic effects (the blue arrow in Fig. 1a, $P_{Hb}$). The $P_{Hb}$ is a distinct characteristic of MNWs because it indicates the magnetic stability of the magnetization related to the spin- and/or orbit-lattice coupling inducing shape and crystal anisotropies. Therefore, it provides a difference in magnetization in the same forward field after starting from two different initial states, or two different backward fields. On the other hand, the reversible switching field (RSF) indicates the instantaneous disturbance in magnetization induced by the immediate fields applied on the MNWs, such as forward field, MNWs interaction field, and para/diamagnetic response of the surroundings. This distinct feature of the project method, discrimination of the RSF and ISF, makes it an excellent method for detection, identification, and quantification of MNWs buried deeply in biological tissues, which cannot be realized by other magnetic characterization methods, such first-order reversal curve (FORC) or hysteresis loop measurements (Fig. 1b and c). Furthermore, since it only measures a few points next to the upper branch of the hysteresis loop rather than scanning the whole hysteresis loop area (as it is done in FORC measurement, Fig. 1b), it is practically very fast which makes it competitive with other detection/identification methods, such as flow cytometry or impedance cytometry methods while nondestructively measuring whole samples.

## Experiments

Two sets of the MNWs were synthesized inside the porous polycarbonate tissues using the electrodeposition technique, Fig. 2. More details regarding the synthesis approach are provided in the ESI.† We chose polycarbonate in this study because polycarbonate is a biocompatible polymer and has been widely used in bone/organ repairing, drug delivery, and tissue regenerative engineering.[40–46] Note all these applications are *in vivo*, besides those, we would like to mention the polycarbonate is a polymer that has been used widely in daily applications, such as covers for cell phones, a great example of skin contact without any toxicity or side-effect. The first set was

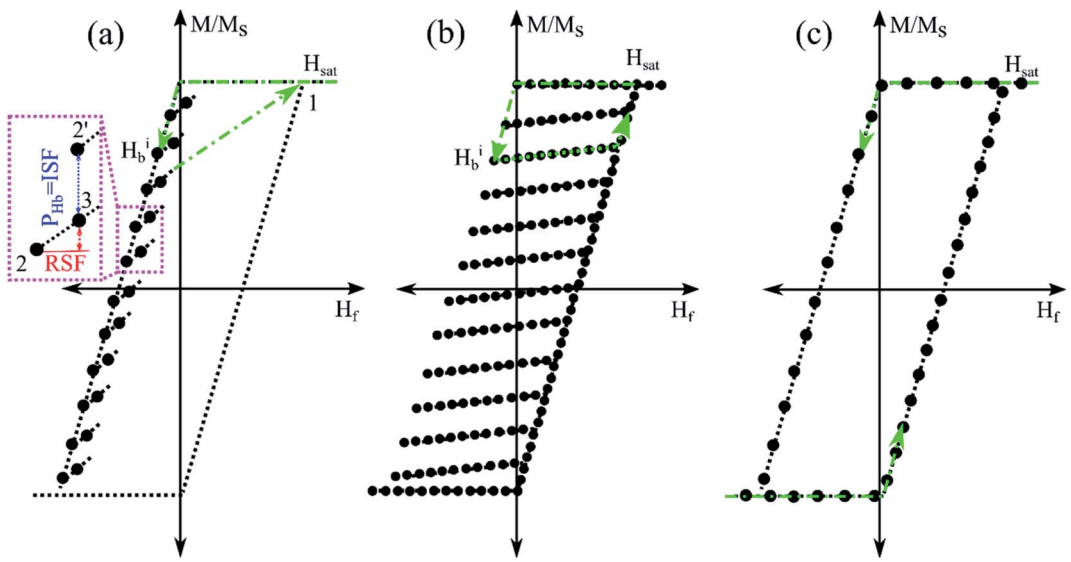


Fig. 1 Schematic illustration of characteristics for MNWs based on the projection method: (a) the collected data points according to the projection method, (b) the collected data points according to the FORC method, and (c) the collected data points according to the hysteresis loop measurement. In subfigure (a), the red arrow shows the reversible switching field (RSF) and the blue arrow shows the irreversible switching field (ISF), which is $P_{Hb}$. In all subfigures, the green arrows show the direction of data acquisition.

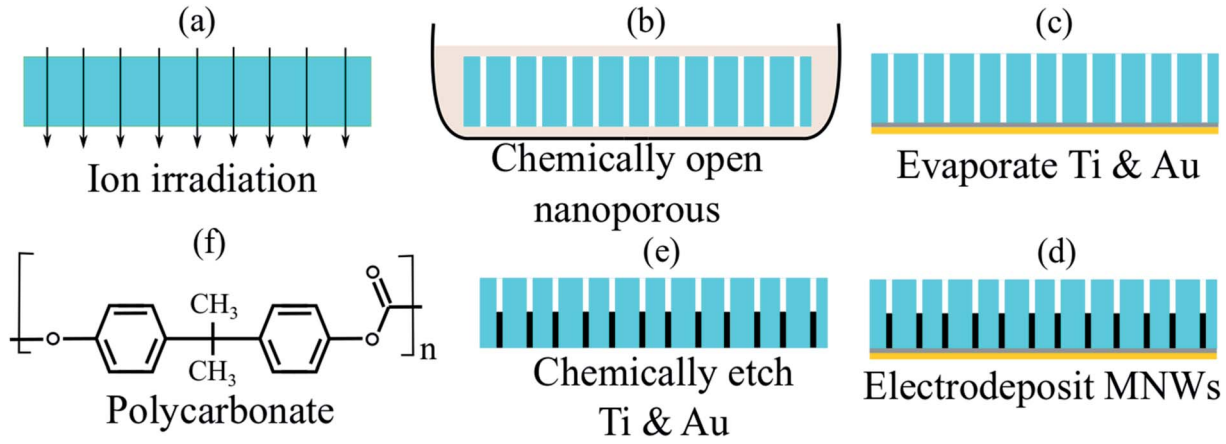


Fig. 2 A schematic depicting MNWs synthesis, dimensions are not drawn to scale. (a) The ion irradiation of a raw polycarbonate foil (blue box), (b) chemical etching (brownish box) of the ion irradiated polycarbonate, (c) evaporating the back contacts to make electrical current, the blue strip is Ti and the yellow strip is Au, (d) electrodepositing the MNWs (black strips), (e) a combination of wet and dry etch process to remove the back contacts, and (f) the chemical structure of polycarbonate.

made of cobalt (Co) and another was made of nickel (Ni). The biocompatibility of the MNWs has been studied in our past studies and other researchers,[22,47–50] we thus did not performed biocompatibility study here. Furthermore, here the Ni and Co MNWs are embedded inside the polycarbonate, thus they will not be in contact with biological entities, such as cells, if they are used *in vivo* applications. Four different types of MNWs were prepared for each set, classified according to their diameters, leading to eight different types of MNW-loaded tissues. To evaluate the accuracy of the projection method for demultiplexing, the diameters and geometrical arrangements were kept the same in each set. These parameters, diameter (inter-wire distance to diameter ratio), were 200 nm (3), 100 nm (7), 50 nm (9), and 30 nm (15).

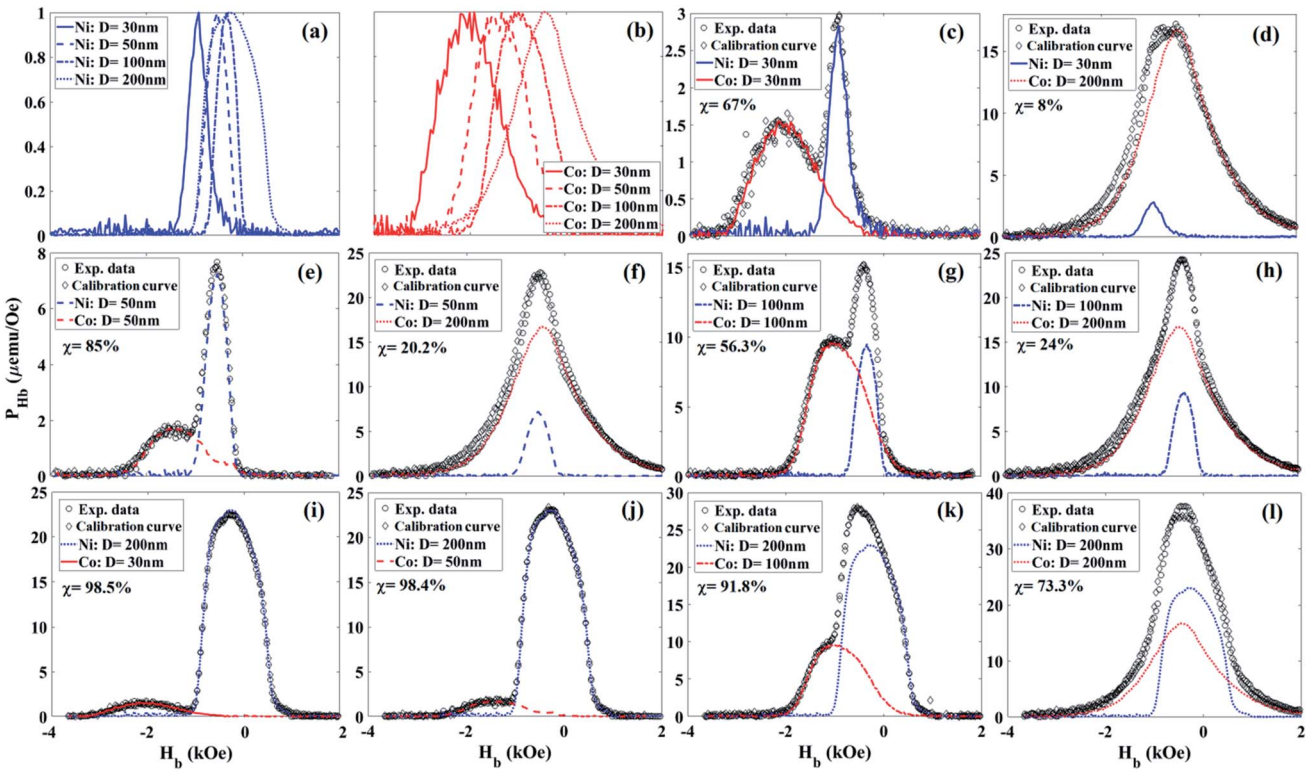


Fig. 3 The projection of the area scanned by the projection method on the backward field, $P_{Hb}$. The black and green lines show the results for the individual Ni MNWs and Co MNWs, respectively, in all subfigures. The "Exp. data" and "calibration curve" are the measured data directly on the combination and the superposition of the individual MNWs $P_{Hb}$, respectively. The subfigures (a) and (b) are the normalized $P_{Hb}$ for the Ni and Co MNWs, respectively, which they are the calibration samples. All subfigures share the same horizontal axis.

 

First, the magnetic characteristics of the individual MNW-loaded tissues were measured and analyzed using the projection method, see ESI.† Next, the magnetic characteristics of combinations of MNW-loaded tissues were measured and compared to those of the individual tissues. Specifically, to analyze the reliability and reproducibility of the projection method for the quantitative description, the individual characteristics were used as calibration curves such that a volume ratio ($\chi$) could be fit for the combinations. The fitting quality was evaluated using the root mean square (RMS) error of the difference between the "experimental data" and "calibration curve", which is the weighted summation of the corresponding parameters of the calibration samples. This RMS error was minimized $\chi$ for each type of MNWs in the combination. More details on the measurements and statistical analysis are given in the ESI.†

## Results

The $P_{Hb}$ was calculated from the experimental data using a theoretical formula, given in the ESI,† and the results are plotted in Fig. 3. As can be seen in Fig. 3, the $P_{Hb}$ maintains fairly sharp features even for very small volume ratios ($\chi$). For example, the $\chi$ of the Co 30 nm and Ni 200 nm combination is only ~1.5% Co (98.5% Ni). $P_{Hb}$ solely relies on the intrinsic properties of the MNWs, such as shape and crystal anisotropies, which determine the average coercivity of each MNWs type. Note the coercivity is the location of the $P_{Hb}$ peak, which is distinct for different types of the MNWs—the coercivities are given in Fig. 5 ESI.† For a comprehensive demultiplexing analysis, we intentionally made both MNWs sets to have moderately overlapping characteristics. The $P_{Hb}$ of combined samples includes the feature of individual MNWs types in the combinations. The distinction of the features depends on the coercivities of the individual MNWs in each combination and on $\chi$. As the $\chi$ increases, having less from one type compared to another, the sharpness of the features decreases too. Therefore, it is essential to have MNWs types with very distinct coercivity in the combination in order to recognize the features for a more accurate $\chi$ measurement. Since the $P_{Hb}$ of a MNW type is independent from others, the identification and quantification can be done by comparing the experimental data from the combination with those of the individual types in the combination using a simple fitting model, see the ESI for more details.†

## Discussion

Fig. 4 shows the quantitative volume ratio ($\chi$) determined using $P_{Hb}$. The $P_{Hb}$ characteristics determined $\chi$ with a reasonable error. The accuracy of the $P_{Hb}$ is directly correlated to the intrinsic properties of the MNWs. Since the projection method eliminates the extrinsic effects by separating the RSF from ISF, the projection method precisely detects, identifies, and quantifies the types and volume ratios of the components inside each combination.

By realizing the $P_{Hb}$ as a reliable and accurate magnetic characteristic, now we compare this with optical techniques that employ optical nanoparticles, such as fluorophore molecules. Optical techniques measure on log scales due to large variance in measurements induced by the photo-instability or background signals. In addition, the fluorescence signals cannot overlap if they are to be demultiplexed, and they are susceptible to bleaching, blurry focusing, and other optical artifacts. Importantly, regardless of the complex and expensive components of optical techniques, there is a huge trade-off between their resolution and speed. For example, to speed up scanning a large area, one must increase the field of view and pixel size which significantly deteriorates the resolution. Interestingly, all of these limitations can be significantly mitigated using the projection method. The projection method can be done on any sample, regardless of its volume or concentration. On other words, the projection method remotely measures the whole sample at once regardless of the surroundings, and it is high-speed compared to the conventional magnetic measurements. Furthermore, the magnetic moments of the MNWs are stable so they can be remotely and noninvasively excited by a single excitation source, a magnetic field.

As shown in the ESI,† the $P_{Hb}$ indeed is the derivative of the magnetization with respect to the $H_b$. The peak of $P_{Hb}$ determines the average coercivity of the MNWs. Furthermore, its width and overall shape are correlated to the standard deviation of the coercivity and the interaction fields among the MNWs. Therefore, we define the specificity of the MNWs as the derivative of the $P_{Hb}$ with respect to $H_b$ ($dP_{Hb}/dH_b$), shown in Fig. 4. That is because the $dP_{Hb}/dH_b$ determines the deformation or variation of the $P_{Hb}$ with respect to the $H_b$. In other words, the $dP_{Hb}/dH_b$ is the curvature of the magnetization that is a unique function of the coercivity distribution and the interaction fields, which are solely depend on the MNWs type, size, and arrangement.

According to Fig. 5, the derivative has two peaks that are symmetric with respect to the coercivity, which is the location of the $P_{Hb}$'s peak, see Fig. 5 ESI.† The symmetry of the peaks significantly improves the ability of the projection method to determine the component type and $\chi$ inside a combination, because it increases the opportunity to have distinct signatures.

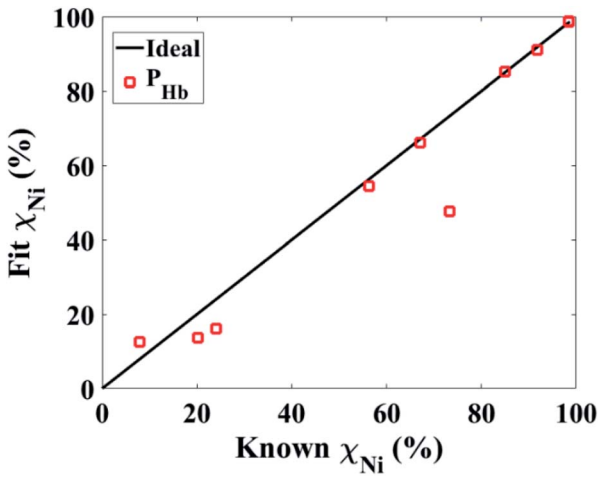


Fig. 4 Comparison of the accuracy of the magnetic characteristics measured by the projection method for quantifying the volume ratios ($\chi$) of the MNWs in combinations.

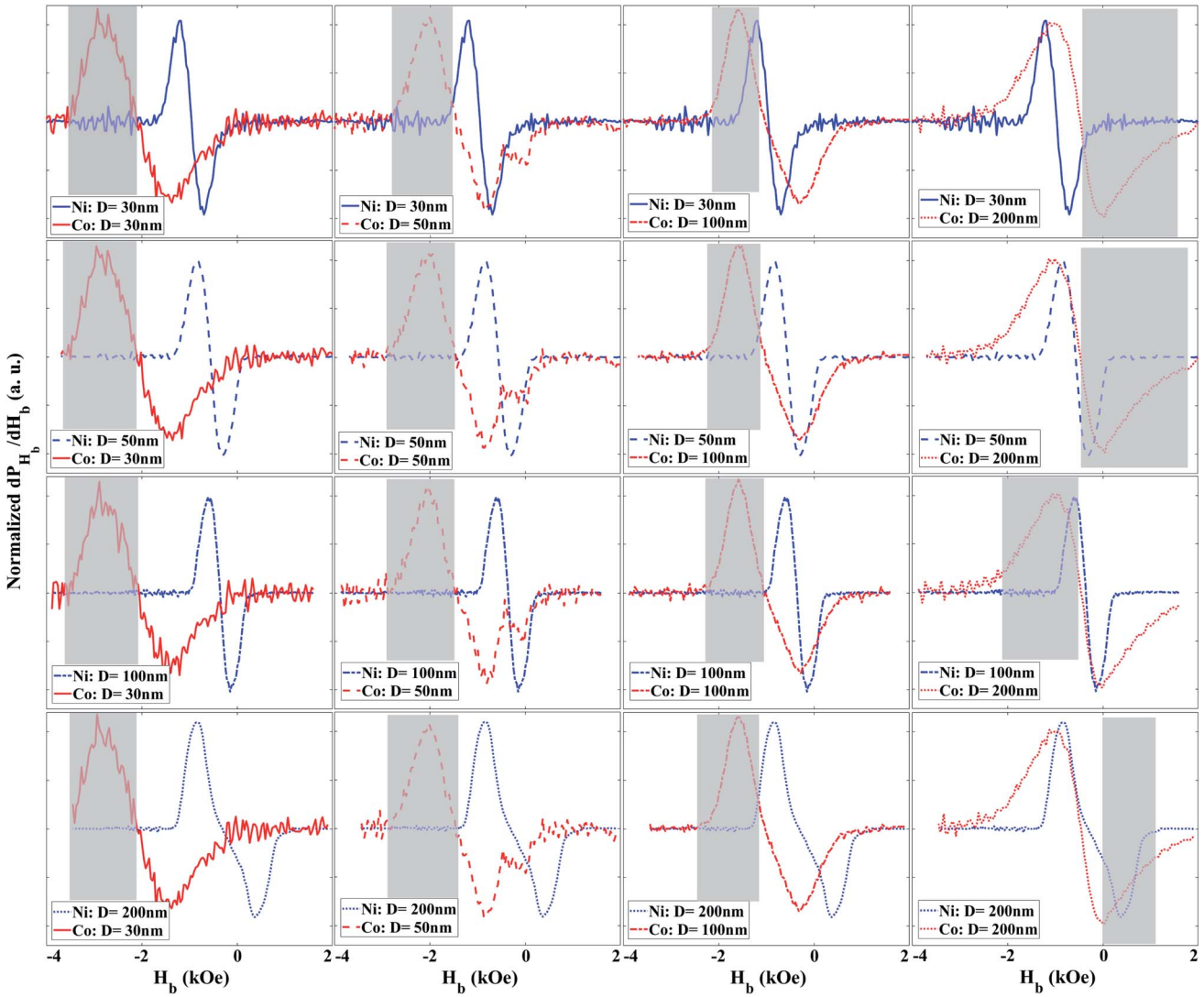


Fig. 5 The characteristic specificity of the MNWs. The grey boxes suggest the most distinct peak that can be used to replicate the second peaks and distinguish the biomarkers. All subfigures share the same horizontal axis.

The intermediate between the peaks, where the $dP_{Hb}/dH_b$ is zero, determines the average coercivity. Moreover, the separation of the peaks is related to the standard deviation of the coercivity and the interaction fields. Since the MNWs are synthesized in the similar polycarbonate templates, it is expected to have similar standard deviation for the coercivity. However, since the Co MNWs have larger crystal anisotropy and magnetic moment compared to the Ni MNWs for the same dimensions, the location of the intermediate point and the distribution of the peaks are different between the Co and Ni MNWs leading to distinguishable signatures for demultiplexing them. Furthermore, for the same material, the coercivity increases as the diameter decreases. For example, changing the diameter from 30 nm to 200 nm moves the intermediate points to smaller $H_b$ values. Therefore, the $dP_{Hb}/dH_b$ can be further engineered by changing the composition and diameters of the magnetic nanowires leading in generating diverse signatures for multiplexing/demultiplexing of the magnetically enriched biological tissues.

The grey boxes in Fig. 5 highlight the range of $H_b$ that can be used to detect one of the MNW biomarker types as distinct from the other, which we could call primary. If one of the secondary MNW peaks is detected (specificity), the other peak can be replicated due to symmetry, such that $\chi$ can be quantified even with an overlapping primary peak. Importantly, distinct peaks can be engineered by careful design of MNW coercivity, which is a function of the magnetic component, size, and aspect ratio (diameter to length). For example, in these combinations, the 200 nm Co tissues did not enable combinations that were demultiplexed with as high confidence as the other combinations. This still means that 12 combinations of 2 tissue types were successful. Further "barcodes" will be possible as this technique is expanded to new MNW-loaded tissues as components for new combinations.

Most biomarker signatures, such as the emission spectra of optical biomarkers, have only one peak and that peak must be distinct from the others. We believe the unique symmetric-peak property of the MNWs, correlated with the projection method

 

and our straightforward analysis, opens a venue towards more accurate and fast multiplexing/demultiplexing of the large volume of biological entities that will fuel the progress of molecular biology, nanomedicine, and medical therapies.

## Conclusion

Here, we proposed a novel magnetic measurement, called the projection method, for accurate and fast quantitative demultiplexing of the MNWs. We showed that the projection method can rapidly and precisely illustrate the unique magnetic characteristics of the MNWs by suppressing the influence of extrinsic effects on intrinsic properties by scanning the vicinity of the upper branch of the MNWs hysteresis loop. Our experimental observations prove that the projection of the switching response on the backward field ($P_{Hb}$), also known as irreversible switching, is a reliable and accurate characteristic for multiplexing/demultiplexing applications. More interesting, its derivative has two peaks that provide more flexibility for generating biomarkers with distinct characteristics compared to optical biomarkers. The $P_{Hb}$ and its derivative have a strong dependence on the intrinsic properties of the MNWs, such as spin-lattice coupling, with minimal extrinsic effects. This finding along with our high-speed measurement protocol for the projection method, 50×–100× faster than the conventional magnetic measurements, makes the projection method competitive to the expensive and complex current state of the art of multiplexing techniques.

## Conflicts of interest

There are not conflicts to declare.

## Acknowledgements

This work is based upon work supported primarily by the National Science Foundation under grant no. CMMI-1762884. Portions of this work were conducted in the Minnesota Nano Center, which is supported by the National Science Foundation through the National Nano Coordinated Infrastructure Network (NNCI) under Award Number ECCS-1542202. Part of this work was performed at the Institute for Rock Magnetism (IRM) at the University of Minnesota. The IRM is a US National Multi-user Facility supported through the Instrumentation and Facilities program of the National Science Foundation, Earth Sciences Division (NSF/EAR 1642268), and by funding from the University of Minnesota. Parts of this work were also carried out in the Characterization Facility, University of Minnesota, which receives partial support from NSF through the MRSEC program.

## References

1 Z. A. Nima, M. Mahmood, Y. Xu, T. Mustafa, F. Watanabe, D. A. Nedosekin, M. A. Juratli, T. Fahmi, E. I. Galanzha, J. P. Nolan, A. G. Basnakian, V. P. Zharov and A. S. Biris, *Sci. Rep.*, 2015, **4**, 4752.

2 L. Zhang, D. Lv, W. Su, Y. Liu, Y. Chen and R. Xiang, *Am. J. Biochem. Biotechnol.*, 2013, **9**, 71–89.

3 E. Martz, *Introduction to Flow Cytometry*, http://www.bio.umass.edu/micro/immunology/facs542/facsprin.htm.

4 J. P. Robinson, *Encycl. Biomater. Biomed. Eng.*, 2004, 922–931.

5 A. Cossarizza, H. D. Chang, A. Radbruch, M. Akdis, I. Andrä, F. Annunziato, P. Bacher, V. Barnaba, L. Battistini, W. M. Bauer, S. Baumgart, B. Becher, W. Beisker, C. Berek, A. Blanco, G. Borsellino, P. E. Boulais, R. R. Brinkman, M. Büscher, D. H. Busch, T. P. Bushnell, X. Cao, A. Cavani, P. K. Chattopadhyay, Q. Cheng, S. Chow, M. Clerici, A. Cooke, A. Cosma, L. Cosmi, A. Cumano, V. D. Dang, D. Davies, S. De Biasi, G. Del Zotto, S. Della Bella, P. Dellabona, G. Deniz, M. Dessing, A. Diefenbach, J. Di Santo, F. Dieli, A. Dolf, V. S. Donnenberg, T. Dörner, G. R. A. Ehrhardt, E. Endl, P. Engel, B. Engelhardt, C. Esser, B. Everts, A. Dreher, C. S. Falk, T. A. Fehniger, A. Filby, S. Fillatreau, M. Follo, I. Förster, J. Foster, G. A. Foulds, P. S. Frenette, D. Galbraith, N. Garbi, M. D. García-Godoy, J. Geginat, K. Ghoreschi, L. Gibellini, C. Goettlinger, C. S. Goodyear, A. Gori, J. Grogan, M. Gross, A. Grützkau, D. Grummitt, J. Hahn, Q. Hammer, A. E. Hauser, D. L. Haviland, D. Hedley, G. Herrera, M. Herrmann, F. Hiepe, T. Holland, P. Hombrink, J. P. Houston, B. F. Hoyer, B. Huang, C. A. Hunter, A. Iannone, H. M. Jäck, B. Jávega, S. Jonjic, K. Juelke, S. Jung, T. Kaiser, T. Kalina, B. Keller, S. Khan, D. Kienhöfer, T. Kroneis, D. Kunkel, C. Kurts, P. Kvistborg, J. Lannigan, O. Lantz, A. Larbi, S. LeibundGut-Landmann, M. D. Leipold, M. K. Levings, V. Litwin, Y. Liu, M. Lohoff, G. Lombardi, L. Lopez, A. Lovett-Racke, E. Lubberts, B. Ludewig, E. Lugli, H. T. Maecker, G. Martrus, G. Matarese, C. Maueröder, M. McGrath, I. McInnes, H. E. Mei, F. Melchers, S. Melzer, D. Mielenz, K. Mills, D. Mirrer, J. Mjösberg, J. Moore, B. Moran, A. Moretta, L. Moretta, T. R. Mosmann, S. Müller, W. Müller, C. Münz, G. Multhoff, L. E. Munoz, K. M. Murphy, T. Nakayama, M. Nasi, C. Neudörfl, J. Nolan, S. Nourshargh, J. E. O'Connor, W. Ouyang, A. Oxenius, R. Palankar, I. Panse, P. Peterson, C. Peth, J. Petriz, D. Philips, W. Pickl, S. Piconese, M. Pinti, A. G. Pockley, M. J. Podolska, C. Pucillo, S. A. Quataert, T. R. D. J. Radstake, B. Rajwa, J. A. Rebhahn, D. Recktenwald, E. B. M. Remmerswaal, K. Rezvani, L. G. Rico, J. P. Robinson, C. Romagnani, A. Rubartelli, B. Ruckert, J. Ruland, S. Sakaguchi, F. Sala-de-Oyanguren, Y. Samstag, S. Sanderson, B. Sawitzki, A. Scheffold, M. Schiemann, F. Schildberg, E. Schimisky, S. A. Schmid, S. Schmitt, K. Schober, T. Schüler, A. R. Schulz, T. Schumacher, C. Scotta, T. V. Shankey, A. Shemer, A. K. Simon, J. Spidlen, A. M. Stall, R. Stark, C. Stehle, M. Stein, T. Steinmetz, H. Stockinger, Y. Takahama, A. Tarnok, Z. G. Tian, G. Toldi, J. Tornack, E. Traggiai, J. Trotter, H. Ulrich, M. van der Braber, R. A. W. van Lier, M. Veldhoen, S. Vento-Asturias, P. Vieira, D. Voehringer, H. D. Volk, K. von Volkmann, A. Waisman, R. Walker, M. D. Ward, K. Warnatz, S. Warth, J. V. Watson, C. Watzl, L. Wegener, A. Wiedemann, J. Wienands, G. Willimsky,

J. Wing, P. Wurst, L. Yu, A. Yue, Q. Zhang, Y. Zhao, S. Ziegler and J. Zimmermann, *Eur. J. Immunol.*, 2017, **47**, 1584–1797.

6 H. KassassirK. SiewieraT. Przygodzki, M. Labieniec-Watala and C. Watala, in *Flow Cytometry – Select Topics*, ed. K.Siewiera, InTech, Rijeka, 2016, ch. 3.

7 S. Bhana, Y. Wang and X. Huang, *Micro Nanosyst.*, 2015, **7**, 1973–1990.

8 M. V. DaCosta, S. Doughan, Y. Han and U. J. Krull, *Anal. Chim. Acta*, 2014, **832**, 1–33.

9 X. Xie, N. Gao, R. Deng, Q. Sun, Q. H. Xu and X. Liu, *J. Am. Chem. Soc.*, 2013, **135**, 12608–12611.

10 M. R. Z. Kouhpanji and B. J. H. Stadler, 2019, **1–9**, arXiv:1911.12480.

11 M. R. Zamani Kouhpanji, J. Um and B. J. H. Stadler, *ACS Appl. Nano Mater.*, 2020, **3**(3), 3080–3087.

12 D. Shi, M. E. Sadat, A. W. Dunn and D. B. Mast, *Nanoscale*, 2015, **7**, 8209–8232.

13 M. Worden, L. Bergquist and T. Hegmann, *RSC Adv.*, 2015, **5**, 100384–100389.

14 C. Iriarte-Mesa, Y. C. López, Y. Matos-Peralta, K. de la Vega-Hernández and M. Antuch, *Top. Curr. Chem.*, 2020, **378**, 12.

15 R. C. Popescu, E. Andronescu and B. S. Vasile, *Nanomaterials*, 2019, **9**, 1–31.

16 J. Um, M. R. Zamani Kouhpanji, S. Liu, Z. Nemati, J. Kosel and B. Stadler, *IEEE Trans. Magn.*, 2020, **56**(2), 1–6.

17 D. Shore, S. L. Pailloux, J. Zhang, T. Gage, D. J. Flannigan, M. Garwood, V. C. Pierre and B. J. H. Stadler, *Chem. Commun.*, 2016, **52**, 12634–12637.

18 Y. S. Jeon, H. M. Shin, Y. J. Kim, D. Y. Nam, B. C. Park, E. Yoo, H.-R. Kim and Y. K. Kim, *ACS Appl. Mater. Interfaces*, 2019, **11**, 23901–23908.

19 J. A. Fernandez-Roldan, D. Serantes, R. P. del Real, M. Vazquez and O. Chubykalo-Fesenko, *Appl. Phys. Lett.*, 2018, **112**, 212402.

20 D. Shore, A. Ghemes, O. Dragos-Pinzaru, Z. Gao, Q. Shao, A. Sharma, J. Um, I. Tabakovic, J. C. Bischof and B. J. H. Stadler, *Nanoscale*, 2019, **11**, 14607–14615.

21 J. Alonso, H. Khurshid, V. Sankar, Z. Nemati, M. H. Phan, E. Garayo, J. A. García and H. Srikanth, *J. Appl. Phys.*, 2015, **117**, 17D113.

22 Z. Nemati, J. Um, M. R. Zamani Kouhpanji, F. Zhou, T. Gage, D. Shore, K. Makielski, A. Donnelly and J. Alonso, *ACS Appl. Nano Mater.*, 2020, **3**, 2058–2069.

23 M. Hoehn, D. Wiedermann, C. Justicia, P. Ramos-cabrer, K. Kruttwig, T. Farr and U. Himmelreich, *J. Physiol*, 2007, **584**, 25–30.

24 J. W. M. Bulte, T. Douglas, B. Witwer, S. C. Zhang, E. Strable, B. K. Lewis, H. Zywicke, B. Miller, P. Van Gelderen, B. M. Moskowitz, I. D. Duncan and J. A. Frank, *Nat. Biotechnol.*, 2001, **19**, 1141–1147.

25 M. Safi, M. Yan, M. A. Guedeau-Boudeville, H. Conjeaud, V. Garnier-Thibaud, N. Boggetto, A. Baeza-Squiban, F. Niedergang, D. Averbeck and J. F. Berret, *ACS Nano*, 2011, **5**, 5354–5364.

26 A. Hultgren, M. Tanase, C. S. Chen, G. J. Meyer and D. H. Reich, *J. Appl. Phys.*, 2003, **93**, 7554–7556.

27 D. E. Shore, T. Dileepan, J. F. Modiano, M. K. Jenkins and B. J. H. Stadler, *Sci. Rep.*, 2018, **8**, 15696.

28 A. Hultgren, M. Tanase, C. S. Chen and D. H. Reich, *IEEE Trans. Magn.*, 2004, **40**, 2988–2990.

29 E. Kaniukov, A. Shumskaya, D. Yakimchuk, A. Kozlovskiy, I. Korolkov, M. Ibragimova, M. Zdorovets, K. Kadyrzhanov, V. Rusakov, M. Fadeev, E. Lobko, K. Saunina and L. Nikolaevich, *Appl. Nanosci.*, 2019, **9**, 835–844.

30 S. Jafari, L. O. Mair, I. N. Weinberg, J. Baker-McKee, O. Hale, J. Watson-Daniels, B. English, P. Y. Stepanov, C. Ropp, O. F. Atoyebi and D. Sun, *J. Magn. Magn. Mater.*, 2019, **469**, 302–305.

31 A. P. Safronov, B. J. H. Stadler, J. Um, M. R. Zamani Kouhpanji, J. Alonso Masa, A. G. Galyas and G. V Kurlyandskaya, *Materials*, 2019, **12**, 2582.

32 A. Sharma, M. D. DiVito, D. E. Shore, A. D. Block, K. Pollock, P. Solheid, J. M. Feinberg, J. Modiano, C. H. Lam, A. Hubel and B. J. H. Stadler, *J. Magn. Magn. Mater.*, 2018, **459**, 176–181.

33 W. Hong, S. Lee, H. Jin, E. Sook and Y. Cho, *Biomaterials*, 2016, **106**, 78–86.

34 H. Lee, M. Choi, J. Lim, M. Jo, J. Han, T. M. Kim and Y. Cho, *Theranostics*, 2018, **8**, 505–517.

35 N. A. Alsharif, A. Martiinez-Banderas, J. Merzaban, T. Ravasi and J. Kosel, *IEEE Trans. Magn.*, 2019, **55**, 1–5.

36 M. Reyes, D. Vickers, K. Billman, T. Eisenhaure, P. Hoover, E. P. Browne, D. A. Rao, N. Hacohen and P. C. Blainey, *Sci. Adv.*, 2019, **5**, 1–10.

37 N. Cummings, R. King, A. Rickers, A. Kaspi, S. Lunke, I. Haviv and J. B. M. Jowett, *BMC Genomics*, 2010, **11**, 641.

38 M. R. Z. Kouhpanji and B. J. H. Stadler, arXiv:2003.06911, 2020, 1–9, https://arxiv.org/abs/2003.06911.

39 M. R. Z. Kouhpanji, P. B. Visscher and B. J. H. Stadler, arXiv:2002.07742, 2020, 1–7https://arxiv.org/abs/2002.07742.

40 S. B. Song, J. W. So, H. S. Ryu and B. S. Kim, *US Pat.*, 2013, 133, 1179–1185.

41 J. Kim, M. H. R. Magno, H. Waters, B. A. Doll, S. McBride, P. Alvarez, A. Darr, A. Vasanji, J. Kohn and J. O. Hollinger, *Tissue Eng., Part A*, 2012, **18**, 1132–1139.

42 R. Glaum, M. Wiedmann-Al-Ahmad, U. Huebner and R. Schmelzeisen, *J. Biomed. Mater. Res., Part A*, 2010, **93**, 704–715.

43 M. N. Ganivada, P. Kumar, P. Kanjilal, H. Dinda, J. Das Sarma and R. Shunmugam, *Polym. Chem.*, 2016, **7**, 4237–4245.

44 C. M. Agrawal and R. B. Ray, *J. Biomed. Mater. Res.*, 2001, **55**, 141–150.

45 J. Liao, L. Zhang, Y. Zuo, H. Wang, J. Li, Q. Zou and Y. Li, *J. Biomater. Appl.*, 2009, **24**, 31–45.

46 A. R. Shrivats, M. C. McDermott and J. O. Hollinger, *Drug Discovery Today*, 2014, **19**, 781–786.

47 A. Sharma, Y. Zhu, S. Thor, F. Zhou, B. Stadler and A. Hubel, *IEEE Trans. Magn.*, 2013, **49**, 453–456.

48 A. Sharma, G. M. Orlowski, Y. Zhu, D. Shore, S. Y. Kim, M. D. DiVito, A. Hubel and B. J. H. Stadler, *Nanotechnology*, 2015, **26**(13), 1–12.

49 P. C. Pinheiro, C. T. Sousa, J. P. Araújo, A. J. Guiomar and T. Trindade, *J. Colloid Interface Sci.*, 2013, **410**, 21–26.

50 S. Schrittwieser, D. Reichinger and J. Schotter, *Materials*, 2018, **11**(1), 45.

 